Photoanodes for Aqueous Solar Cells: Exploring Additives and Formulations Starting from a Commercial TiO2 Paste

Photoanodes for Aqueous Solar Cells: Exploring Additives and Formulations Starting from a Commercial TiO_2 Paste

Dr. Lucia Fagiolari,[a,*] Dr. Matteo Bonomo,[b] Alessio Cognetti,[a] Dr. Giuseppina Meligrana,[a] Prof. Dr. Claudio Gerbaldi,[a] Prof. Dr. Claudia Barolo,[b,*] Prof. Dr. Federico Bella[c,*]

[a] *GAME Lab, Department of Applied Science and Technology, Politecnico di Torino, Corso Duca degli Abruzzi 24, 10129 – Torino, Italy*
[b] *Department of Chemistry, NIS Interdepartmental Centre and INSTM Reference Centre, Università degli Studi di Torino, Via Pietro Giuria 7, 10125 – Torino, Italy*
[c] *Department of Applied Science and Technology, Politecnico di Torino, Corso Duca degli Abruzzi 24, 10129 – Torino, Italy*
Corr. authors: lucia.fagiolari@polito.it; claudia.barolo@unito.it; federico.bella@polito.it

Abstract

While the commercialization of dye-sensitized solar cells (DSSCs) is finally proceeding taking advantage of their low cost and tunable optical features, such as colour and transparency for both indoor and building-integrated applications, the corresponding aqueous counterpart is still at its infancy. Being the TiO_2 electrode a fundamental component for hybrid solar cells, this work investigates the effect of several molecular (α-terpineol, propylene carbonate) and polymeric (polyethylene oxide, polyethylene glycol, carboxymethyl cellulose and xanthan gum) additives when introduced in a commercial TiO_2 paste for DSSCs, conceived for screen-printing (or doctor blade). Among all, the addition of polyethylene glycol leads to the best cell performances, with markedly increased short-circuit current density (+18%) and power conversion efficiency (+48%) with respect to the pristine (commercial) counterpart. When further explored at different concentration levels, electrodes fabricated from polyethylene glycol-based pastes show different morphologies, thicknesses and performances, that are here investigated through (photo)electrochemical, structural, physical-chemical and microscopic techniques.

Keywords

Aqueous electrolyte; Dye-sensitized solar cell; PEG; TiO_2 paste; Water-based electrolyte.

Introduction

In the current climate crisis scenario, the production of energy from renewable sources is one of the main challenges that scientists are facing.[1] Because of the abundance and worldwide distribution of solar light radiation, photovoltaics (PV) is surely one of the suitable solutions to face the current and future energy demand.[2] In this regard, dye-sensitized solar cells (DSSCs) represent a particular type of sunlight converters, being low cost, highly transparent, with tunable colors and with the unique property of harvesting also scattered photons.[3] Due to these intriguing features, DSSCs started to be marketed in the recent years both in the field of architectural integration and in that of portable electronics; the market value was estimated to be 49.6 M$ in 2014 and is estimated to grow at a compound annual growth rate of over 12% from 2015 to 2022.[4]

Since O'Regan and Grätzel reported the first DSSC with a power conversion efficiency (PCE) ≈7%,[5] the highest published value has already reached 14.3%,[6] while the certified record is 12.3%.[7] However, it must always be taken into account that the electrolyte solution of these devices always contains organic solvents, leading to several constrains and issues, *i.e.* volatility, flammability and toxicity. This results in poor long-term stability, high environmental impact and risks for final users.[8] In such a context, the scientific community recently started to spend many efforts towards the replacement of organic solvents-based electrolytes with alternative water-based ones.[9] In addition, the jellification of aqueous electrolytes has recently been proposed to boost the long-term stability of the devices, through (possibly biosourced) polymeric matrices.[10] They are able to entangle the liquid (aqueous) electrolyte, limiting its evaporation and leakage, also facilitating cell assembly and sealing. On the other hand, the electrode/electrolyte interface must be properly tailored to assure an effective penetration of the electrolyte in the mesoscopic semiconductor.

In the whole organic-based DSSCs story, lots of experimental approaches have been developed to tailor the morphology, thickness and photoelectrochemical behavior of TiO_2 electrodes.[11] Conversely, the strategies developed for aqueous cells are very few. Dong *et al*. carried out an octadecyltrichlorosilane post-treatment of the sensitized TiO_2; in this way, dye-free sites were

encapsulated by an insulating layer to avoid unfavorable side reactions promoted by the oxidized redox mediator.[12] Xiang *et al.* proposed TiO_2 nanoparticles-based photoanodes bearing mesoporous TiO_2 beads scattering layers, simultaneously achieving a better light harvesting and a lower diffusion resistance of the quasi-solid electrolyte within TiO_2 beads.[10a] W-doped TiO_2 mesoporous nanobeads were proposed by Guo *et al.*, reaching high surface area and superior scattering effect, as well as a positive shift of the TiO_2 conduction band leading to an enhanced driving force for electron injection.[13] Son *et al.* optimized an atomic layer deposition protocol to post-treat photoanodes, making the otherwise hydrophobic dye-coated surface hydrophilic, thus enhancing photoelectrode pore-filling with aqueous electrolytes.[14]

As an alternative route, the modification of commercial TiO_2 pastes could be a valuable strategy since they are already industrially scaled-up in the DSSCs field, even if the optimization is carried out only for organic solvents-based devices. The average particles dimension is 18 nm, the formulation is conceived to be deposited by screen printing, and a final thickness of 5-6 μm (when using a 43T mesh screen) with high transparency is obtained at the end of the thermal treatment. When working with aqueous quasi-solid electrolytes (hydrogels), two further issues must be considered with respect to the traditional commercial paste: i) to prepare an electrode surface being highly wettable by water; ii) to allow the permeation of hydrogel-based electrolytes in the electrode bulk.[15]

Herein, we propose a study of the effects promoted by different polymeric (*i.e.* xanthan gum, polyethylene oxide, carboxymethyl cellulose and polyethylene glycol) and molecular (*i.e.* α-terpineol and propylene carbonate) species added to the commercial 18NR-T paste by Greatcell Solar (formerly Dyesol), one of the TiO_2 pastes most used in the scientific literature; we adopted the simple doctor-blade deposition method, easily accessible in all laboratories and very close to the industrial printing process. When thermally treated, these additives burn in air, leading to the formation of precise morphologies and thickness values to the resulting TiO_2 electrodes. After a preliminary investigation, we focused our attention on polyethylene glycol, *i.e.* the additive leading to the most efficient devices.

This system was further investigated in depth through chemical-physical approach, in both liquid and quasi-solid state devices.

Experimental section

Materials

NaI, I_2, chenodeoxycholic acid (CDCA), carboxymethyl cellulose (CMC), propylene carbonate (PC), polyethylene glycol (PEG, M_w = 200 g mol^{-1}), polyethylene oxide (PEO, M_w = 400 000 g mol^{-1}), xanthan gum (XG), α-terpineol (TP), $TiCl_4$, H_2PtCl_6, acetone, ethanol, acetonitrile and *tert*-butanol were purchased from Merck and used without further purification. TiO_2 paste 18NR-T was purchased from Greatcell Solar. Milli-Q® water (18 MΩ cm at 25 °C) was obtained with a Direct-Q® 3 UV purification system (Merck Millipore). Sensitizing dye 2-[{4-[4-(2,2-diphenylethenyl)phenyl]-1,2,3,3a,4,8b-hexahydrocyclopento[b]indole-7-yl}methylidene] cyanoacetic acid (D131) was purchased from Inabata Europe SA. Meltonix 1170-60 thermoplastic films and F-doped SnO_2 (FTO) conductive glasses, with sheet resistance of 7 Ω sq^{-1}, were purchased from Solaronix.

Preparation of TiO_2 pastes

For preliminary studies, an amount of 20 wt% of CMC, PC, PEG, PEO, XG or TP was added to the commercial TiO_2 paste, mechanically mixed and magnetically stirred overnight to achieve a homogeneous composition.

As regards the investigation carried out on PEG-based pastes, PEG amounts of 5, 10, 20, 30, 40 and 50 wt% were explored, following the same experimental procedure described above.

Preparation of electrolytes

Milli-Q® water was saturated with CDCA, *i.e.* an excess of CDCA was suspended in water and stirred at 40 °C overnight. Then, after cooling the solution at room temperature, the excess of CDCA was filtered by a filter paper. As regards liquid state devices, NaI and I_2 were added to the CDCA-saturated

solution up to a concentration equal to 3 M and 20 mM, respectively. For quasi-solid state cells, 3 wt% XG was added to the I^-/I_3^- solution, that was then stirred overnight at room temperature, leading to the formation of a hydrogel not flowing when the vial was manually turned upside down.

Fabrication of aqueous DSSCs

FTO glasses were cut into 2 cm × 1.5 cm sheets and used as substrates for both photoanodes and counter-electrodes fabrication. They were cleaned by sonication in water/soap suspension, acetone and ethanol for 10 min each. Commercial and modified TiO_2 pastes were deposited by doctor blade using a 55 µm-thick scotch tape, then dried in air for 20 min and thermally treated at 300 °C for 15 min and at 450 °C for 30 min, to allow the evaporation of the organic compounds of the TiO_2-based formulation. Doctor blade was chosen as deposition method to achieve homogeneous surfaces and avoid the sucker effect often encountered in screen printing processes. $TiCl_4$ treatment was carried out by immersing the TiO_2 electrodes into a $TiCl_4$ 40 mM water solution at 70 °C for 30 min. Then, the electrodes were annealed at 500 °C for 30 min. As regards the sensitization step, $TiCl_4$-treated anodes were dipped into a D131 solution (D131 0.5 mM, CDCA 12.5 mM, in acetonitrile:*tert*-butanol 1:1) for 4 h, then washed with acetone to remove the excess of dye and dried by an air flux.

Counter-electrodes were prepared by thermal decomposition of H_2PtCl_6. 20 µL of a solution consisting of H_2PtCl_6 5 mM in 2-propanol were deposited (twice) on FTO glasses, dried in air and thermally treated at 450 °C for 30 min.

For the liquid state devices, a hole was created in the Meltonix 1170-60 thermoplastic frame (internal area 0.6 cm × 0.6 cm, 60 µm-thick). Photoanodes and counterelectrodes were faced and fixed by hot pressing at 97 °C for 15 s. Then, the liquid electrolyte solution was injected by a vacuum backfilling process. The hole was sealed by using a commercial epoxy glue. Conversely, in the case of hydrogel-based devices, 1.6-1.7 mg of quasi-solid electrolyte were deposited on photoanodes.[15] Then, they were faced to counterelectrodes using the Meltonix 1170-60 thermoplastic film as both spacer and sealant, subsequently hot pressed at 97 °C for 15 s.

For each experimental condition, at least four devices were fabricated and characterized. Errors are indicated in this manuscript by means of the standard deviation.

Characterization techniques

The viscosity behaviour and rheological properties of the pastes were examined by a rheometer Discovery HR1 (TA Instruments) equipped with plate/plate geometry (diameter 20 mm, gap 200 μm). Temperature control (20 ± 0.1 °C) was obtained by a Peltier plate. Measurements were conducted for 180 s in order to obtain a stable viscosity value.[16]

UV-Vis transmittance of both sensitized and unsensitized photoanodes was measured in the range 300-800 nm by a Cary 300 UV-Vis spectrophotometer.

Contact angle was measured by a DSA100 drop shape analyzer (Krüss GmbH), depositing a 5 μL water drop and without waiting for relaxation time.

X-ray diffraction (XRD) was performed by a Panalytical's X'Pert^3 MRD PRO diffractometer, equipped with a Cu K_α X-ray source and a curved graphite secondary monochromator. Since anatase and SnO_2 peaks are very close in the spectra, TiO_2 pastes were deposited onto a Cu support, followed by thermal treatment and XRD measurement.

Cross-sectional field emission scanning electron microscopy (FESEM) was carried out by an Auriga Zeiss instrument (Carl Zeiss). It was couple with an energy dispersive X-ray (EDX) spectrometer, model QUANTAX (Bruker), operating with resolution of 123 eV (Mn K_α).

Profilometry was carried out by a Dektak 150 surface profiler (Veeco Instruments Inc.).

As regards PV characterization, J-V curves were recorded by using a Keithley SourceMeter® kit and a VeraSol-2 LED solar simulator (class AAA, by Oriel®), calibrated with an Oriel® PV reference cell system (model 91150V). Usually, 45 s were required to reach stable results, in terms of short-circuit current density (J_{sc}), open-circuit voltage (V_{oc}), fill factor (FF) and overall photoconversion efficiency (PCE).

Electrochemical impedance spectroscopy (EIS) curves were recorded by using a CH760D potentiostat (CH Instruments, Inc.) under 1 sun illumination conditions.

Stability test were performed by storing the cells under dark condition and at room temperature, measuring the J-V curve every week.

Results and discussion

Effect of different additives on cells performance

In order to understand the effect of different additives (introduced in the commercial TiO_2 paste) on the performance of the resulting photoanodes, an amount of 20 wt% of these polymeric (PEG, CMC, XG, PEO) and molecular (TP, PC) species was introduced in the pristine sample. The choice of these additives was motivated to their widespread use in current DSSCs manufacturing, where they are introduced to achieve peculiar features. In particular, PEO, XG, CMC, PC and PEG are widely used for the preparation of quasi-solid and solid polymer electrolyte-based devices.[17] TP is a solvent typically used in commercial TiO_2 pastes optimized for standard DSSCs prepared by screen-printing processes;[18] in addition, it finds application as solvent in pastes used for the deposition of C-based substrates[19] and composite materials.[20] PC and PEG show similar rheological behavior to TP, but they have been used mostly for the preparation of low-volatility electrolytes; in particular, PEG at M_w = 200 g mol^{-1} was chosen due to its viscosity, this latter being roughly equal to that of TP.[21] Overall, all of these compounds represent cost-effective commodities in the DSSCs industry, easy to be integrated for the fabrication of TiO_2 electrodes and then used in aqueous devices. As regards the amount (*i.e.*, 20 wt%), it was chosen since it could likely lead to a detectable effect on cells performance.

All pastes prepared in this work were mechanically mixed and stirred to achieve a homogeneous formulation. Both the pristine and modified pastes were used to prepare photoanodes by the doctor blade method (this latter being available in all academic laboratories and compatible with screen-printable pastes) and, finally, sintered and $TiCl_4$-treated; average thicknesses ≈4.3 μm were obtained

(by cross-section FESEM measurements) independently from the additive used. Lab-scale DSSCs were assembled using D131 dye as sensitizing molecule and liquid or gel aqueous electrolytes (see Experimental Section).

Before starting the analysis of the results, it should be pointed out that the adopted approach consists of a wide and rapid screening of different additives, useful to identify evident clear effects on PV performance. This must not be confused with the traditional multivariate approach that is used by companies to formulate commercial products,[22] that surely leads to a wider exploration of the experimental domain, but at a different cost in terms of both chemicals and time. Table 1 highlights the effect of each additive introduced into the commercial paste on the PV performance of the resulting DSSCs; the percentage values indicate how each PV parameter varies with respect to pristine condition, *i.e.* the batch of cells assembled with the unmodified commercial paste. The effect of each additive on the PV performances depended on the aggregation state (*i.e.*, liquid or quasi-solid) of the electrolyte sandwiched between cell electrodes. This led us to figure out that photoanode surface wettability and electrolyte penetration in the nanostructure were two factors that could play the leading role and being affected by the TiO_2 paste composition; both of them will be analyzed later in the manuscript.

Table 1 Effect of different additives introduced in the TiO_2 commercial paste on PV parameters of the resulting lab-scale aqueous DSSCs. The comparison is made versus the pristine devices, featuring these PV values: 0.61 ± 0.01 V, 4.4 ± 0.4 mA cm^{-2}, 0.58 ± 0.05, 1.5 ± 0.1% for the liquid cell; 0.61 ± 0.02 V, 4.6 ± 0.7 mA cm^{-2}, 0.66 ± 0.04, 1.8 ± 0.3% for the quasi-solid cell.

		PC	**PEG**	**CMC**	**XG**	**TP**	**PEO**
Liquid electrolyte	V_{oc}	+7% (± 0.2)	+4% (± 0.2)	+6% (± 0.2)	+5% (± 0.2)	+4% (± 0.2)	+3% (± 0.2)
	J_{sc}	+21% (± 0.2)	+18% (± 0.1)	–4% (± 0.1)	–1% (± 0.09)	–3% (± 0.1)	–28% (± 0.07)
	FF	+19% (± 0.3)	+22% (± 0.2)	+4% (± 0.2)	+19% (± 0.3)	+15% (± 0.2)	+9% (± 0.2)
	PCE	+51% (± 0.1)	+48% (± 0.09)	+8% (± 0.1)	+25% (± 0.07)	+18% (± 0.1)	–10% (± 0.05)
Quasi-solid electrolyte	V_{oc}	+2% (± 0.4)	+4% (± 0.4)	+5% (± 0.4)	–2% (± 0.6)	+2% (± 0.4)	+2% (± 0.4)
	J_{sc}	–3% (± 0.2)	+12% (± 0.2)	–4% (± 0.2)	–27% (± 0.2)	–1% (± 0.2)	–15% (± 0.2)
	FF	+3%	+5%	+3%	+1%	+2%	+3%

		(± 0.1)	(± 0.2)	(± 0.1)	(± 0.05)	(± 0.05)	(± 0.1)
	PCE	+3% (± 0.2)	+23% (± 0.2)	+5% (± 0.2)	–27% (± 0.2)	–1% (± 0.2)	–9% (± 0.2)

Granular and non-volatile XG led to a positive effect (+25%) when used for liquid state devices, while a strong reduction in PCE (–27%) was measured in the presence of the hydrogel electrolyte. We hypothesize that this polysaccharide (industrially used as thickening and stabilizer agent and derived from the fermentation process by *Xanthomonas campestris*) created a certain porosity in the TiO_2 electrode; these pores were easily filled by the liquid solution, but the penetration of the hydrogel electrolyte was not successful; this is reflected in the important decrease of J_{sc} values.

PEO had an overall negative effect, with a drop in PCE values of 10% and 9% in the presence of liquid and gel electrolytes, respectively; in both cases, this was caused by a markedly worsened J_{sc}. CMC showed an almost neutral (slightly positive) effect in both cases. Overall, it must be stated that solid state additives (XG, CMC and PEO) formed less homogeneous and processable pastes; even after prolonged and vigorous stirring, some grains were still present in the final pastes and the resulting electrodes (obtained through the doctor blade technique) showed little inhomogeneities at first visual inspection (see Figure S1 in the Supporting Information).

As regards liquid molecular additives, PC and TP showed a positive effect only when the liquid electrolyte was used, while an appreciable effect on PV performances was not detected in the presence of the quasi-solid state mediator. Contrary to what observed with solid polymeric additives, PC and TP made the TiO_2 paste less dense. However, the dilution of the commercial paste was too intense and brought to a more difficult deposition by doctor blade; indeed, it was difficult to obtain a perfectly homogeneous layer after sintering.

Among all liquid additives, only PEG clearly showed a remarkable positive effect in both liquid and gel electrolytes, with an increase in PCE values of +48% and +23%, respectively, due to the simultaneous improvement of J_{sc} and V_{oc} values. From a practical point of view among all pastes,

PEG-based ones were those characterized by the best doctor blade processability and perfect homogeneity of the printed and sintered films (see Figure S2 in the Supporting Information).

Characterization of photoanodes obtained by PEG-based pastes

To further understand the main features of photoanodes obtained from PEG-based pastes and justify their remarkably higher efficiency with respect to the pristine counterparts, an in-depth characterization was carried out. The commercial TiO_2 paste was mixed with different (six) amounts of PEG: 5, 10, 20, 30, 40 and 50 wt%; the main aim was that of studying the effect of different additive concentrations on the morphological, structural and PV features of the resulting electrodes. The PEG-based TiO_2 pastes showed perfect rheological features to be used for the doctor-blade process; the addition of PEG led to lower viscosity values, as shown in Figure S3 in the Supporting Information**.** First, XRD patterns were recorded (after thermal and $TiCl_4$ treatments) in order to identify any possible (even if not expected) change in the crystal structure of the electrodes. Figure 1 reveals that the addition of PEG (at any concentration, 50 wt% is shown as representative for all samples) did not modify the crystal structure of TiO_2. Indeed, TiO_2 was always present in the anatase polycrystalline phase: the diffraction patterns clearly revealed peaks at 25.3°, 37.7°, 48.0 and 55.1°, corresponding to the (101), (004), (200) and (211) crystal planes (JCPDS card number #89-4921), respectively. However, PEG-based TiO_2 pastes led to a different ratio between (004) and (101) peaks; in particular, this ratio increased upon PEG addition. In the metal oxides field, this is usually accompanied by the elongation of crystals along the *c*-axis direction,[23] and the images taken by electron microscopy (shown in the following paragraphs) will confirm this trend. Notice that not indexed peaks present in the patters are those belonging to Cu (the substrate used for doctor-blading the TiO_2 pastes) or CuO/Cu_2O (originated from the oxidation of Cu during the sintering process in air). Even the ratio among these peaks varies in the two patterns shown in Figure 1; although there is no reference in the literature, we assume that what observed is due to a PEG-promoted effect on Cu foil oxidation process during the thermal treatment.

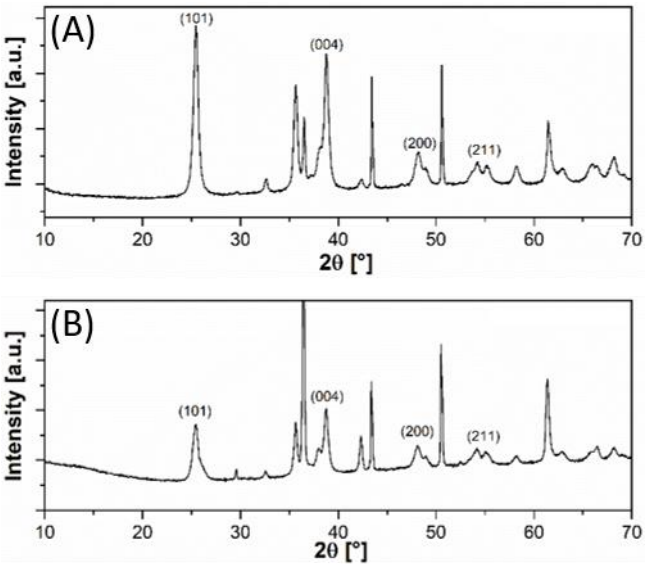

Figure 1 XRD patterns of electrodes obtained from (A) pristine and (B) 50 wt% PEG additivated TiO_2 pastes. Samples were deposited onto a Cu foil as a substrate and then annealed as described in the Experimental Section.

SEM micrographs showed that different PEG amounts in the TiO_2 paste caused appreciable differences on the surface morphology of the electrodes. As shown in Figure 2, the pristine, 5 and 10 wt% PEG-modified pastes, once thermally treated, led to porous surfaces, characterized by a regular morphology (large void spaces were not detected). On the other hand, when a 20 wt% PEG-based paste was used, voids with sub-micrometric dimension started appearing (Figure 2D). The dimension of these latter increased at higher PEG amounts, up to what observed for the sample coming from the 50 wt% PEG-based paste: cavities of about 500 nm are clearly visible in the micrograph (Figure 2G). The creation of even more voids was attributed to the presence of higher amounts of this low molecular weight oligomer, that - during the thermal process - burnt leaving cavities in the semiconductor film; this was even more pronounced if – at high PEG content – PEG pools were formed as local inhomogeneities. In this context, PEG acted as a pore-forming agent able to lead to a suitable nanostructured electrode for DSSC, *i.e.* porous enough to allow the penetration of the electrolyte, but not too porous to affect the area of the electrode/electrolyte interface, which represents the core of the photoelectrochemical phenomenon in these cells.

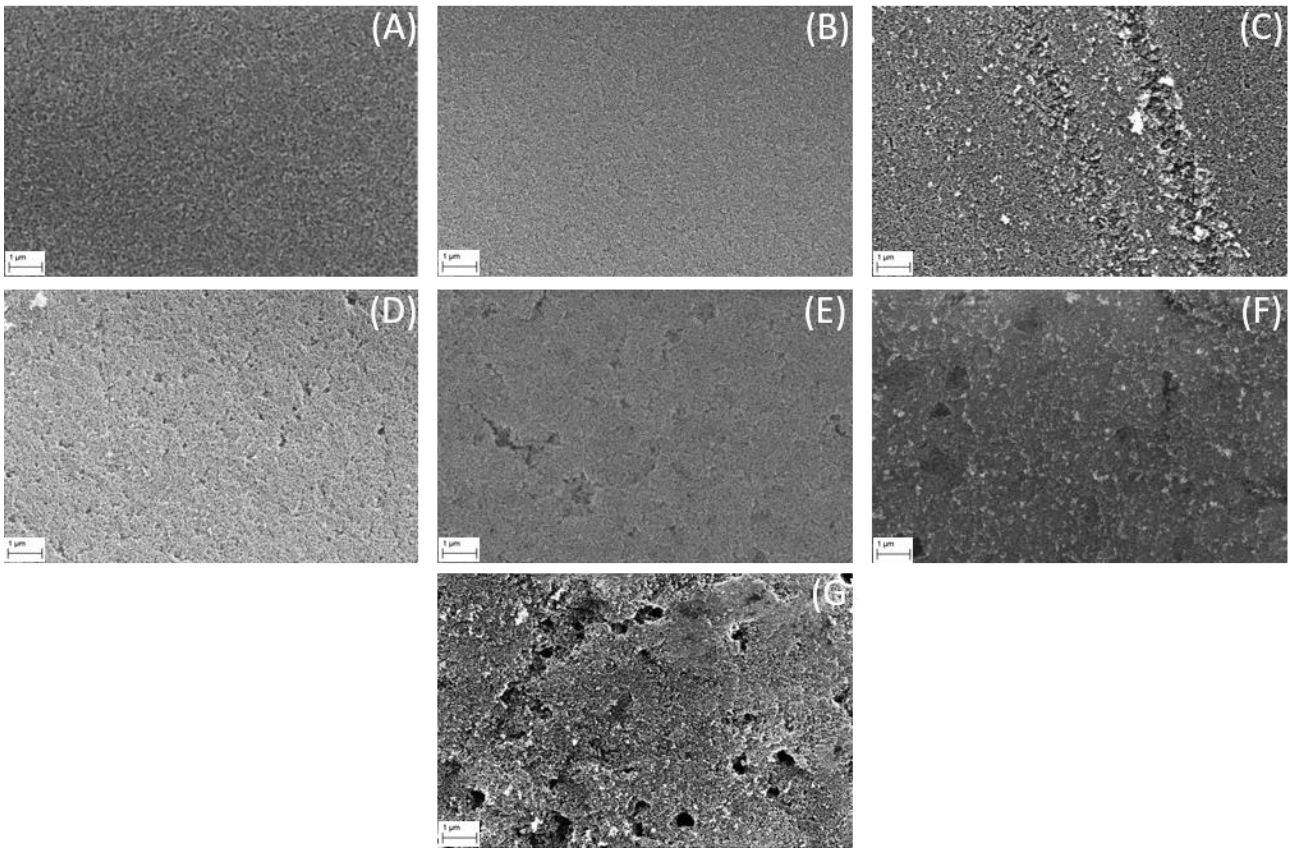

Figure 2 Top-view SEM images of TiO_2 electrodes prepared from (A) pristine, (B) 5, (C) 10, (D) 20, (E) 30, (F) 40 and (G) 50 wt% PEG-based pastes deposited on FTO substrates and thermally annealed.

It would surely be interesting to correlate the surface area of the electrodes with the amount of additive present in the corresponding pastes. However, this is not of easy (and rational) realization at a laboratory scale. Indeed, considering the density of anatase (3.78 g cm^{-3}), it is easy calculating that a standard DSSC photoanode (area: 0.25 cm^2; thickness: 6 μm) contains no more than 5.67×10^{-4} g of active material. This means that to achieve 1 g (the amount necessary for BET analysis) of doctor-bladed TiO_2 with the same thickness (and overall properties) of that used for DSSCs, we should have covered (and then scratched away for the subsequent BET analysis) a substrate area of 441 cm^2, *i.e.* 1764 electrodes like those used in this work. Therefore, we continued our investigation by a qualitative approach through electron microscopy.

Cross-sectional FESEM micrographs (shown in Figure 3) reveal that the bare TiO_2 paste led to the formation of spherical particles with a diameter of 18-20 nm (other micrographs are given in Figure S4 in Supporting Information). On the other hand, elongated TiO_2 nanoparticles were detected in samples derived from 50 wt% PEG-based paste. Therefore, a first aspect became clear: PEG addition did not modify the crystallographic structure of the electrodes, but their morphology changed. A similar effect is known, in the DSSCs field, for other compounds, such as terpineol and ethylcellulose, that were proposed as morphology-controlling additives in TiO_2 screen-printable pastes.[18] From the cross-sectional FESEM micrographs, thickness values of 7-8 μm and 8-9 μm were measured for samples derived from pristine and 50 wt% PEG-based pastes, respectively. We also measured the thickness values of the whole sample series through profilometry, and the resulting trend in shown in Figure 4A. Here, data follow a reverse bell-shaped curve. As regards the sample derived from the pristine TiO_2 paste, the nominal thickness of 6 μm was ensured (equal to that obtainable by screen-printing the same paste, accordingly to the technical data sheet). With the addition of PEG, the resulting thickness started decreasing, reaching a minimum value of 4 μm for the sample derived from 20 and 30 wt% PEG-based pastes. Such a thickness reduction was attributed to the shrinkage of the active material; indeed, the organic additive evaporated during the thermal treatment, leaving back cavities that, subsequently, were filled by TiO_2 nanoparticles. However, when samples coming from 40 and 50 wt% PEG-based pastes were measured through profilometry, an increase of thickness values was detected up to 4.9 and 6.6 μm, respectively. In this case, the shrinkage of the material did not happen, but the hollow structure left after PEG evaporation was preserved during the thermal sintering. This was also confirmed by the presence of large cavities observed from electron microscopy micrographs.

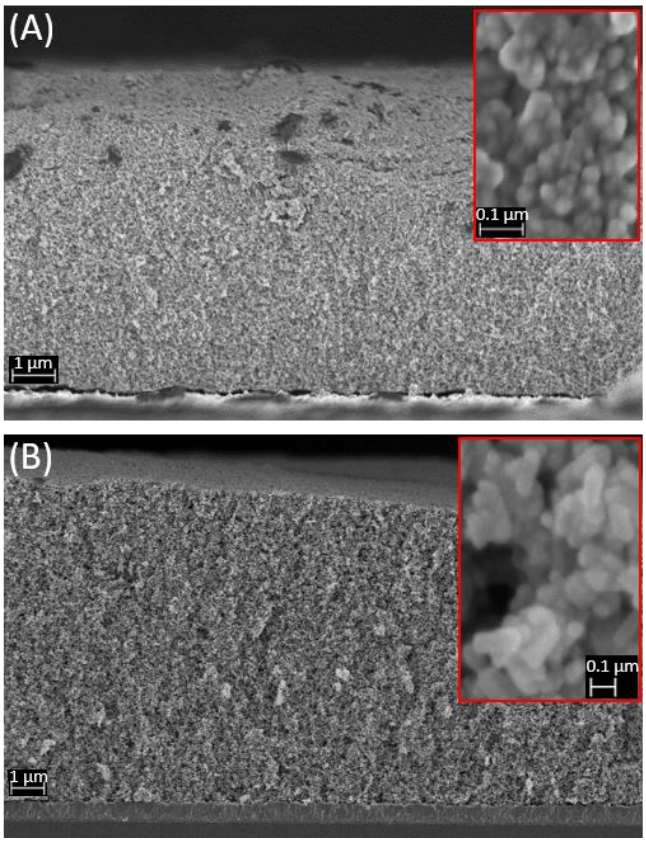

Figure 3 Cross-sectional FESEM micrographs of TiO_2 electrodes prepared from (A) pristine and (B) 50 wt% PEG-based pastes deposited on FTO substrates and thermally annealed.

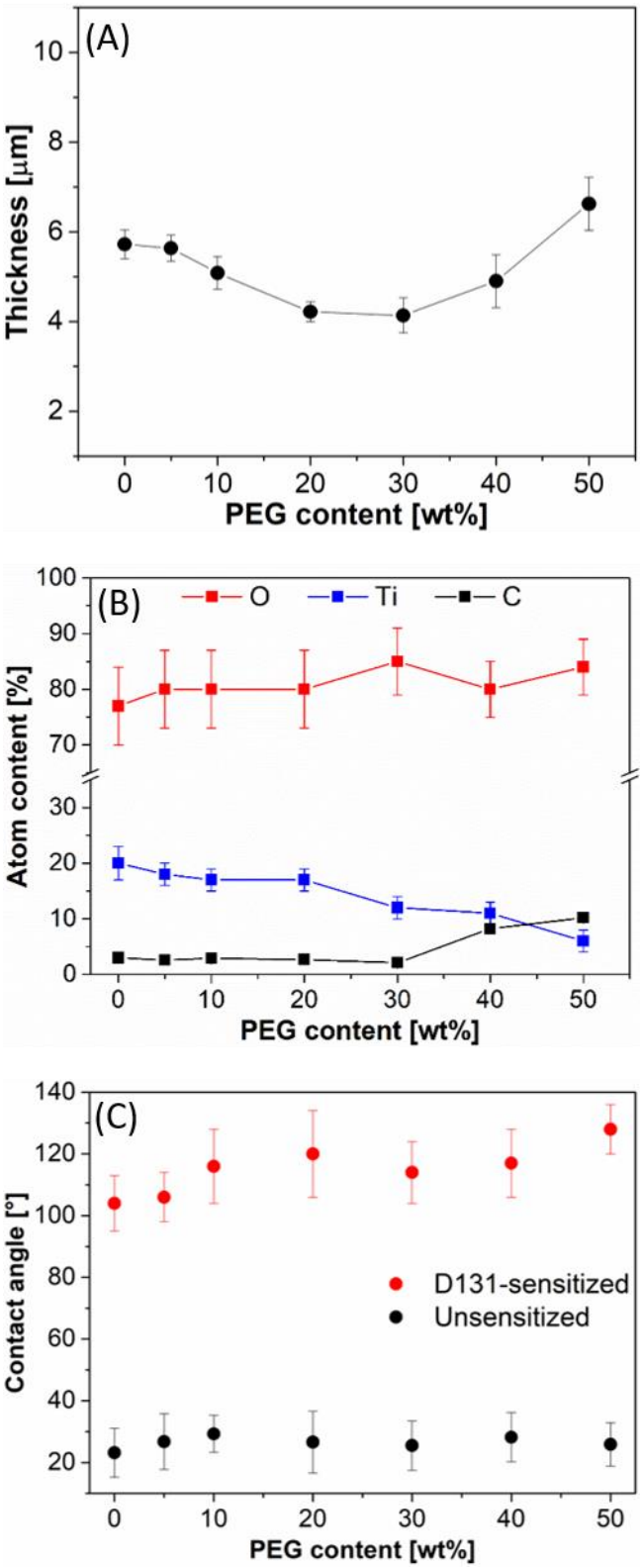

Figure 4 (A) Thickness of TiO_2 electrodes obtained from pastes containing different amounts of PEG. (B) Atomic composition (from EDX) of TiO_2 electrodes *vs.* PEG content of the pastes used for the doctor blade process. (C) Contact angle of unsensitized and dye-sensitized photoanodes (after $TiCl_4$ treatment), prepared with different TiO_2-based pastes. Contact angle was recorded soon after the deposition of the water drop, without waiting for relaxation.

The ratio between Ti, O and C atoms was determined by EDX to evaluate whether PEG residuals (or organic moieties coming from its decomposition) were still present in the thermally treated electrodes. As shown in Figure 4B, the relative content of Ti decreased while raising the PEG amount in the paste; on the other hand, C content was found to increase, in particular for electrodes obtained from 40 and 50 wt% PEG-based pastes. This suggested that, in these electrodes, some PEG (or any organic residues coming from its degradation) was still present after the annealing. We should also remind that a C amount of ≈5% (or lower) is common in these studies, due to the atmospheric contamination during samples processing. As regards O content, it was quite constant when different pastes were used; in fact, in these electrodes O can come from both TiO_2 and PEG.

UV-Vis transmittance spectra (Figure S5 in Supporting Information) were recorded in order to quantify the transparency of the photoelectrodes and to verify any variation caused by the different composition of pastes (and resulting electrodes). Figure S5A in Supporting Information shows the transmittance spectra of unsensitized photoanodes. It is noteworthy that photoanodes obtained with the commercial, 5 and 10 wt% PEG-based pastes were the most transparent of the whole series, with a transmittance of almost 35% in the visible range. Then, the transmittance started to decrease for electrodes prepared from 20 and 30 wt% PEG-based pastes and was dramatically reduced for higher PEG contents. This trend was attributed to the presence of cavities in these electrodes, able to lead to light interference phenomena, thus decreasing the overall transmittance.[24] This effect was also easily visible at human eye, as shown in Figure S5C in Supporting Information. Transmittance spectra of dye-sensitized photoanodes (Figure S5B in Supporting Information) followed the same trend of the unsensitized ones. In these cases, all samples showed a transmittance reduction in the range from 350 to 450 nm, due to the presence of the chemisorbed D131 molecules. Photoanodes derived from 40 and 50 wt% PEG-based pastes evidenced a stronger reduction of transmittance in the visible region with respect to the other photoanodes of the series. This phenomenon was reasonably attributed to a major adsorption of D131 molecules in the form of multilayers or aggregates in the bigger pores present in those electrodes.

Finally, contact angle measurements (Figure 4C) were performed in order to evaluate the wettability of the photoelectrodes, characterized by different composition, thickness and morphology. Contact angle values were measured soon after the deposition of the water drop, without waiting for drop relaxation (that was, in turns, very fast). Contact angles of unsensitized photoanodes were very low, ranging from 20 to 30°. These low values reflected the strong hydrophilicity of unsensitized TiO_2, and relevant differences between electrodes obtained from different pastes were not observed, suggesting that the addition of PEG did not influence the photoanode wettability. Conversely, contact angles of dye sensitized-photoanodes were markedly higher, reflecting the hydrophobicity of the D131 dye. In this case, and differently with respect to what observed for unsensitized electrodes, a small increase in the contact angle values appeared when PEG was introduced (and its amount progressively increased) in the TiO_2 pastes. With reference to the two data series shown in Figure 4C, the only explanation that can justify the observed trend is that an increase in dye loading occurred as the quantity of PEG present in the TiO_2 paste increased.

Photovoltaic characterization of DSSCs assembled with photoanodes obtained from PEG-based pastes

Electrodes obtained with modified TiO_2 pastes and sensitized with D131 were used as photoanodes for lab-scale aqueous DSSCs. Pt-coated FTO glasses and I^-/I_3^- were used as counter-electrodes and redox shuttle, respectively. J-V curves of aqueous DSSCs were recorded under 1 sun (AM 1.5G) illumination by a LED-powered solar simulator.

Table ***2*** and Figure 5 list the PV parameters obtained (with relative errors) for the different batches of cells.

Table 2 PV parameters of aqueous DSSCs assembled with the photoanodes obtained from different PEG-based pastes. Cells were measured under 1 sun illumination (AM 1.5 G).

	PEG [wt%]	**V_{oc} [V]**	**J_{sc}**	**FF**	**PCE [%]**

			[mA cm^{-2}]		
Liquid electrolyte	0	0.61 ± 0.01	4.4 ± 0.4	0.58 ± 0.05	1.5 ± 0.1
	5	0.64 ± 0.01	4.7 ± 0.2	0.70 ± 0.01	2.1 ± 0.1
	10	0.64 ± 0.02	4.9 ± 0.4	0.69 ± 0.01	2.2 ± 0.1
	20	0.64 ± 0.01	5.2 ± 0.3	0.69 ± 0.01	2.3 ± 0.1
	30	0.64 ± 0.01	4.0 ± 0.6	0.71 ± 0.01	1.8 ± 0.3
	40	0.65 ± 0.02	3.4 ± 0.4	0.68 ± 0.02	1.5 ± 0.2
	50	0.62 ± 0.06	3.2 ± 0.6	0.68 ± 0.03	1.4 ± 0.3
Quasi-solid electrolyte	0	0.61 ± 0.02	4.6 ± 0.7	0.66 ± 0.04	1.8 ± 0.3
	5	0.64 ± 0.01	4.6 ± 0.4	0.68 ± 0.03	2.0 ± 0.2
	10	0.63 ± 0.02	4.6 ± 0.9	0.68 ± 0.06	2.1 ± 0.3
	20	0.64 ± 0.01	5.1 ± 0.5	0.71 ± 0.01	2.3 ± 0.2
	30	0.63 ± 0.01	4.3 ± 0.5	0.70 ± 0.01	1.9 ± 0.2
	40	0.64 ± 0.01	4.0 ± 0.8	0.71 ± 0.01	1.8 ± 0.4
	50	0.63 ± 0.01	3.1 ± 0.2	0.69 ± 0.01	1.4 ± 0.1

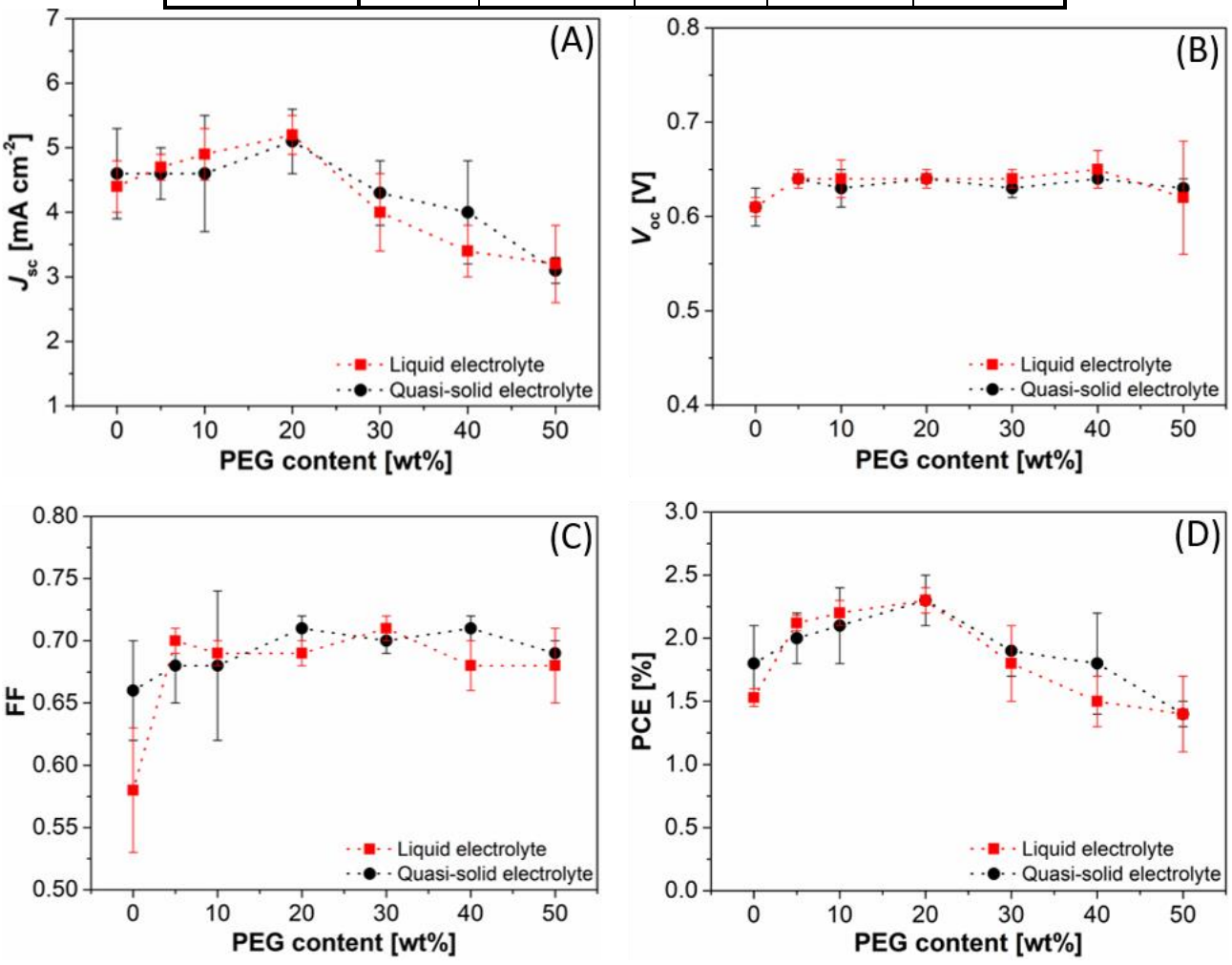

Figure 5 PV parameters of aqueous DSSCs assembled with the photoanodes obtained from different PEG-based pastes. Cells were measured under 1 sun illumination (AM 1.5 G).

In general, substantial differences in terms of current and efficiency between liquid and quasi-solid state electrolytes were not found. PV parameters were almost comparable between these two types of electrolytes, suggesting that the polymeric matrix of the gel ensured a good charge transport and did not hinder the redox shuttle ions motion.[15] As evidenced in Figure 5, J_{sc} and PCE trends followed a similar trend, where it emerged that the devices assembled with photoanodes prepared from the 20 wt% PEG-based paste achieved the best efficiency, both with liquid and quasi-solid state electrolytes. The corresponding average PV parameters under 1 sun irradiation were: J_{sc} = 5.2 mA cm^{-2}, V_{oc} = 0.64 V, FF = 0.69 and PCE = 2.3% for the cell based on the liquid electrolyte; J_{sc} = 5.1 mA cm^{-2}, V_{oc} = 0.64 V, FF = 0.71 and PCE = 2.3% for the cell based on the quasi-solid state electrolyte. In both liquid and quasi-solid state devices, V_{oc} was quite constant upon the explored PEG content values introduced into the commercial TiO_2 paste, suggesting that the thermodynamic energy level of the conduction band of TiO_2 did not change upon the imposed photoanode modification. Anyway, V_{oc} values measured for cells assembled with photoanodes prepared from PEG-based pastes were always higher with respect to the pristine devices. Actually, the effect of PEG on the final electrode morphology and surface properties led to an overall inhibition of recombination phenomena at the photoanode/electrolyte interface. J_{sc} and, consequently, PCE increased with the introduction of PEG up to 20 wt%. When higher amounts of PEG were mixed with the commercial TiO_2 paste, J_{sc} and PCE decreased and reached lower values than those measured for pristine TiO_2 electrodes. We hypothesize that the large voids present in both 40 and 50 wt% PEG-based electrodes did not properly work in the DSSC scheme, due to both the formation of multilayer and/or aggregates of D131 dye molecules and the presence of residuals of PEG (or its decomposition residues) after the thermal treatment.

PV parameters were also measured under different irradiation conditions (see Figure 6) in order to evaluate the linearity of J_{sc} (and eventually PCE) as a function of the simulated sunlight intensity. On one side, V_{oc} and FF were quite constant with the irradiation power; conversely, J_{sc} values linearly increased while passing from 0.2 to 1 sun irradiation, no matter the nature of the electrolyte: this

means that significant diffusion limitations of the redox shuttle did not take place in our PV systems; the same occurred for cells assembled with pristine electrodes. Overall, PCE was almost independent from the irradiation power and this represents a not common observation in the DSSCs field, where typically PCE increases when the irradiation intensity is lowered.[25] Indeed, a simultaneous improvement of FF is often detected when going toward weaker sunlight, due to the lower impact of cell components resistance when few charges pass through the device. This is not the case of our work, where we were able to achieve high FF values (≥0.70) already at 1 sun and, due to thermodynamic reasons, it could not be boosted even more when decreasing the irradiation power. Overall, a FF ≈0.70 for a lab-scale aqueous solar cell measured under 1 sun irradiation represents a very good achievement and a solid basis for future advances in this field.

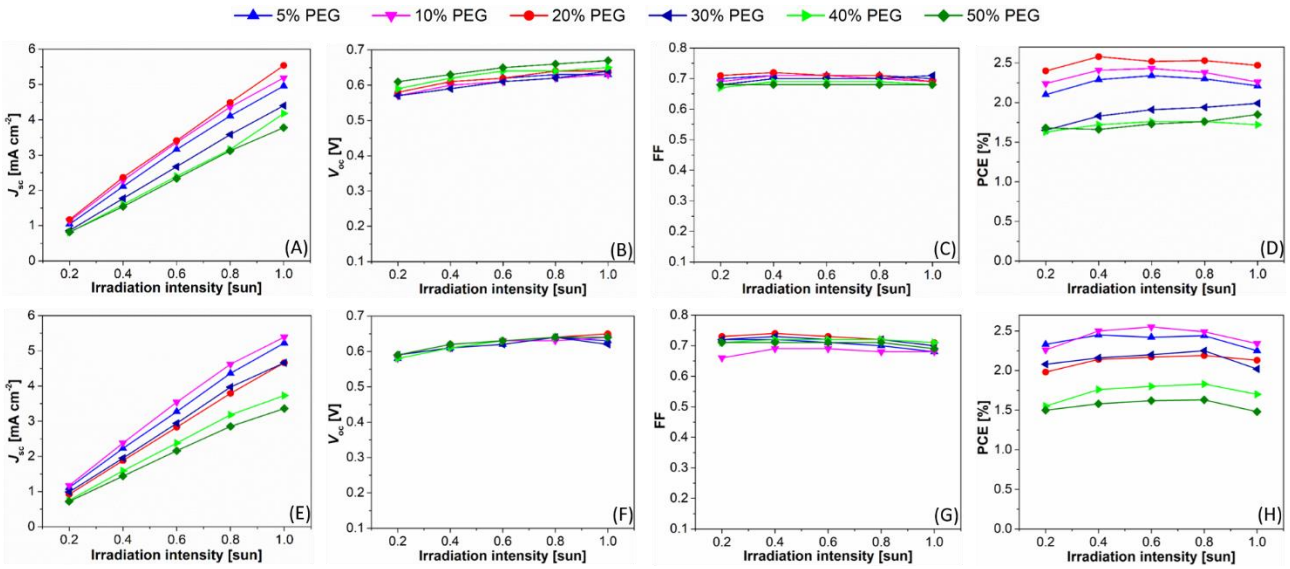

Figure 6 PV parameters of aqueous DSSCs assembled with the photoanodes obtained from different PEG-based pastes. Cells were measured under different light intensities (0.2-1 sun), using both (A-D) liquid and (E-H) quasi-solid state electrolytes.

Long-term stability was assessed storing the cells under dark at room temperature and measuring PV parameters under 1 sun irradiation upon time. In many cases, as shown in Figure 7, the best efficiency was reached after roughly 10 days. This was ascribed to the slow kinetic of the photoanode wetting; it was a common fact for both liquid and quasi-solid state electrolytes, and it has been often observed in our previous studies on aqueous DSSCs.[10b] This phenomenon was detected also by other research

groups[26] and must be carefully considered when writing and reading literature articles on the topic of aqueous photovoltaics. From the comparison between Figure 7A and Figure 7B, it emerges that the use of the hydrogel electrolyte strongly increased the stability of the resulting lab-scale devices. 80 days (*i.e.*, an aging time much longer with respect to those typically found in the literature, *viz.* 10-40),[27] the normalized PCE was 0.85 for the most stable cell (PEG 5 wt%) and 0.63 for the less stable one (pristine TiO_2 electrode). The polymeric matrix of the XG entrapped the solvated redox shuttle, successfully limiting its evaporation and leakage from the device; this is clearly shown in Figure S6 in the Supporting Information, where J_{sc} is the only PV parameter affected upon time. As regards the TiO_2 paste used, it is clear that the addition of PEG led to more stable cells in the presence of both liquid and quasi-solid state electrolytes. Indeed, in both cases the cells fabricated using the pristine TiO_2 paste resulted to be the least stable. Considering that the efficiency loss of these lab-scale DSSCs is attributed to electrolyte leakage (from the electrolyte layer and, consequently, from the photoanode nanostructure), we can assume that the morphology obtained when using PEG-based TiO_2 pastes improves the electrolyte retention within the photoanode.

Figure 7A also shows a wide difference among the aging profile of liquid state cells fabricated from different TiO_2 pastes. Indeed, using TiO_2 pastes containing large amounts of PEG led to a markedly reduced stability: after 80 days, their normalized PCE ranged from 0.16 to 0.50. On the other hand, liquid cells fabricated using lower amounts of PEG for photoanode preparation were more stable, with a loss of efficiency ranging from 19% to 24%. This was justified considering that, in our experimental setup, we inject a fixed amount of liquid/quasi-solid electrolyte; therefore, if the electrode contains many void spaces in its bulk (and this is the case of electrodes prepared with large amounts of PEG), these can trap a high electrolyte quantity, making it not available in the rest of the cell volume (*i.e.*, between the electrodes and at the electrolyte/Pt interface).

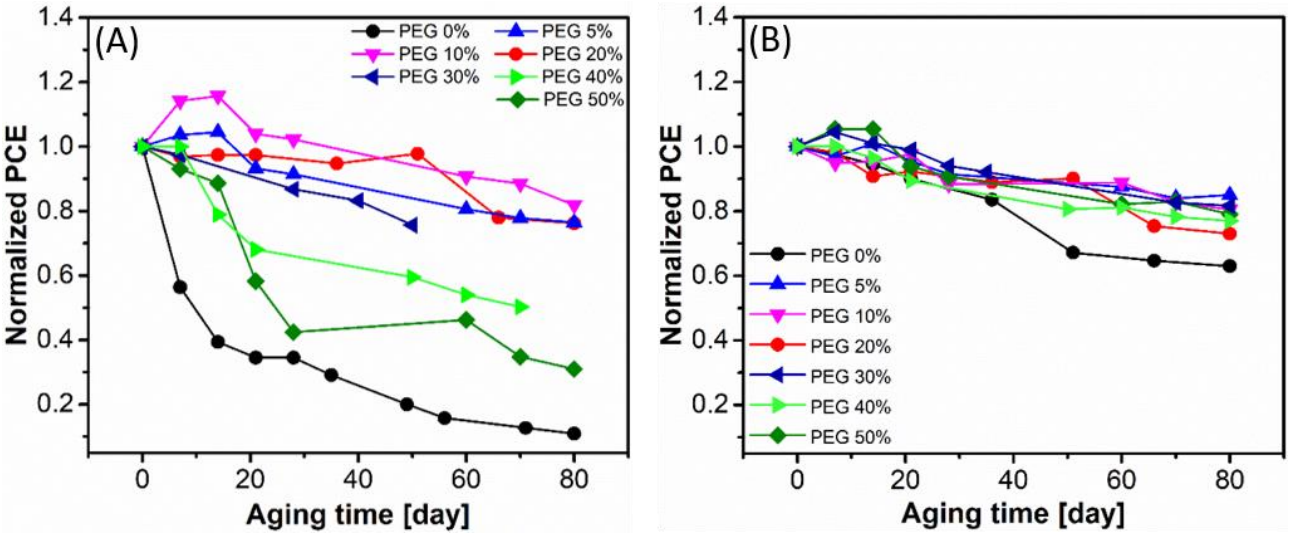

Figure 7 Long-term stability of aqueous DSSCs assembled with (A) liquid or (B) quasi-solid state electrolytes. Normalized efficiency for cells assembled with photoanodes obtained from different PEG-based pastes is shown. During aging, cells were stored under dark and at room temperature.

Electrochemical characterization of DSSCs assembled with photoanodes obtained from PEG-based pastes

In order to deeply understand the effect of the addition of PEG into the TiO_2 paste, we performed electrochemical impedance measurements (under illumination and with a superimposed polarization, *i.e.* the V_{oc} of each device). The impedance spectra of both liquid and quasi-solid devices are shown in Figure 8. In these spectra, the first (partially hidden) semicircle could be ascribed to the electrolyte regeneration at the counterelectrode. The bigger semicircle is due to the recombination process at the (sensitized) photoanode/electrolyte interface. The latter semicircle (at lower applied frequencies) is ascribable to the diffusion resistance of the electrolyte, that is usually higher in aqueous DSSCs compared to the classical organic solvents-based devices.[28] Experimental data interpolated by the equivalent circuit depicted in Figure S7 in the Supporting Information, where R1 is the series resistance, R2 and C2 are the photoanode/electrolyte interface resistance (R_{CT}) and chemical capacitance of the photoanode (C_{μ}), respectively. R3 and C3 are the charge transfer resistance and capacitance at the counterelectrode/electrolyte interface, whereas W3 is Warburg element, accounting for the diffusion of the redox mediator throughout the electrolyte. It is worth mentioning that,

compared to an organic solvents-based device, an aqueous DSSC shows a slower diffusion of the redox shuttle, being the diffusion coefficient of I_3^- smaller than that in organic media,[29] *e.g.* acetonitrile or 3-methoxypropionitrile.

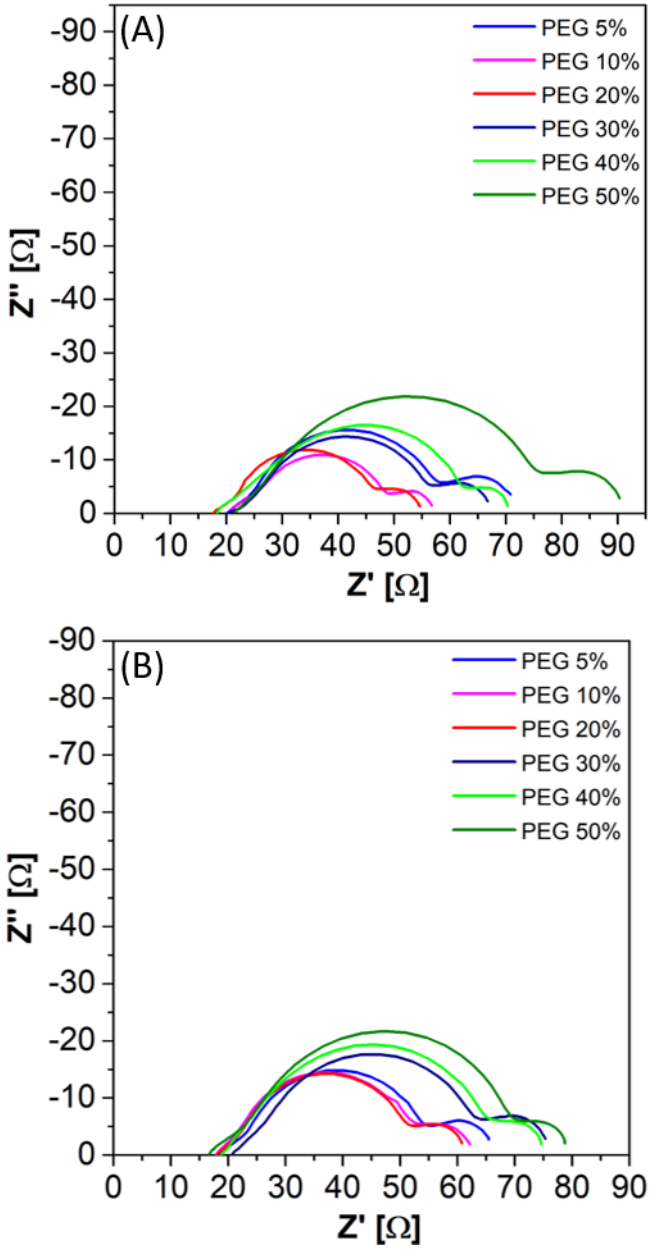

Figure 8. EIS spectra of (A) liquid and (B) quasi-solid state aqueous DSSCs assembled with photoanodes obtained from different PEG-based pastes. Spectra were recorded under 1 sun irradiation and the equivalent circuit used in shown in Figure S7 in the Supporting Information. Representative Nyquist plots with fitted experimental data are shown in Figure S8 in the Supporting Information.

Looking at the EIS spectra, a clear trend could not be evidenced for liquid devices. On the other hand, hydrogel-based counterparts evidenced a counterintuitive behavior, being the less efficient device (*i.e.* PEG 50 wt%) the one showing the biggest semicircle. Indeed, a bigger semicircle is usually associated to a higher recombination resistance and, thus, to a more performing device. It is worth mentioning that in the present case two factors should be considered throughout the analyses of the EIS spectra. First of all, the photoanodes have different thicknesses and the resistance values obtained from the interpolation procedure should be scaled accordingly. Secondly, the equivalent circuit employed for fitting the experimental data (Figure 8C) did not embed the transmission line element (the fitting did not converge); consequently, a separation between R_{rec} and R_t (*i.e.*, the charge transport resistance throughout the photoanode) was not possible. This means that a smaller semicircle could both due to a less resistive film (*i.e.*, smaller R_t, desired behavior) or to a more probable recombination phenomenon (*i.e.*, smaller R_{rec}, unwanted feature). In this context, we employed R2 as the convolution between R_{rec} and R_t. Furthermore, R2 was normalized for the thickness of each electrode.

In Table 3 and Table 4 we summarize the values of different EIS parameters obtained from the fitting procedure for liquid and polymeric devices, respectively. As already evidenced above, a clear trend in the R2 value could not be depicted. Indeed, R2 seemed to become smaller with the electrode thinning (see Figure 4A). This allowed us to hypothesize that, in the present case, R2 was mainly ruled by the transport resistance. Anyway, a thorough analysis of the general EIS scenario of aqueous DSSCs falls outside the scope of the present work and it will be discussed in a forthcoming paper. As expected, the only parameter being substantially influenced by the change in the physical status of the electrolyte was the resistance of the Warburg element, being the latter more resistive for quasi-solid electrolytes compared to the liquid counterparts. We could easily ascribe the slower diffusion process (associated to higher W3 resistance) to the more viscous nature of the XG matrix. Furthermore, regardless of the nature of electrolyte, a sharp increase of the Warburg resistance was experienced when the PEG content in the paste was higher than 30 wt%. We tentatively justify this evidence by considering the formation of bigger voids in the photoanodes that could partially trap

larger volume of electrolyte, thus leading to a decreased amount of effectively available redox mediator. As mentioned above, aqueous DSSCs require a longer activation period with respect to the non-aqueous counterparts; in this regard, we are investigating a reversible sealing systems to allow a re-fill of the aqueous electrolyte (both liquid or quasi-solid) after a couple of weeks. This would also allow the replacement of the electrolyte migrated from the inter-electrodic volume to the void spaces present in the photoanode bulk.

Table 3 Interpolated parameters obtained from the fitting of the EIS spectra of liquid electrolyte-based aqueous DSSCs, assembled with photoanodes prepared from different PEG-based pastes. For each value the associated error is lower than 5%.

	PEG 5 wt%	**PEG 10 wt%**	**PEG 20 wt%**	**PEG 30 wt%**	**PEG 40 wt%**	**PEG 50 wt%**
R1 [Ω]	20.4	20.4	17.7	21.1	18.4	21.3
R2 [Ω]	46.8	46.1	40.5	54.5	42.2	50.9
C2 [F]	0.004	0.005	0.005	0.005	0.006	0.006
R3 [Ω]	2.8	2.8	2.7	2.6	2.8	2.6
W3 [Ω]	25.9	24.4	27.1	33.5	37.1	50.9
C3 [mF]	0.035	0.066	0.045	0.052	0.061	0.077

Table 4 Interpolated parameters obtained from the fitting of the EIS spectra of quasi-solid state electrolyte-based aqueous DSSCs, assembled with photoanodes prepared from different PEG-based pastes. For each value the associated error is lower than 5%.

	PEG 5 wt%	**PEG 10 wt%**	**PEG 20 wt%**	**PEG 30 wt%**	**PEG 40 wt%**	**PEG 50 wt%**
R1 [Ω]	18.7	18.0	18.2	20.7	18.9	17.5
R2 [Ω]	75.6	56.8	45.6	50.0	51.5	74.9
C2 [F]	0.004	0.004	0.006	0.005	0.005	0.003
R3 [Ω]	3.1	2.1	1.8	3.3	2.9	4.3
W3 [Ω]	33.9	33.0	32.2	38.2	44.1	50.1
C3 [mF]	0.030	0.066	0.044	0.049	0.055	0.032

To shed more light on these properties, we plotted the EIS data also in the Bode's shape (*i.e.*, angle phase as a function of applied frequencies, see Figure 9). In this case, the main peak is ascribable to the sole recombination phenomena. The frequency of the maximum point is inversely proportional to the lifetime of electron diffusing throughout the photoanode. Straightforwardly, higher frequency of

the maximum point was related to faster recombination process and less performing devices. As regards the electron lifetime (*i.e.*, the averaged time the electrons injected in the TiO_2 could move throughout the photoanode before occurring in recombination reactions) for liquid state cells, the slower time (21.7 mS) was obtained for cells assembled with photoanodes coming from 30 wt% PEG-based paste, and similar values were also associated to PEG 5-20 wt% samples (21, 17.5 and 19.3 mS, respectively). Very interestingly, shorter times were calculated for PEG 40 wt% (13.0 ms) and PEG 50 wt% (11.4 ms) samples. These values accounted for the worse photoelectrochemical performances of the corresponding lab-scale devices, despite the higher R2 obtained from the interpolation of EIS data. A similar trend could be highlighted considering the hydrogel-based devices: the electron lifetime values were 18.7, 19.0, 21.4, 22.1, 16.1 and 14.1 ms upon increasing PEG amounts.

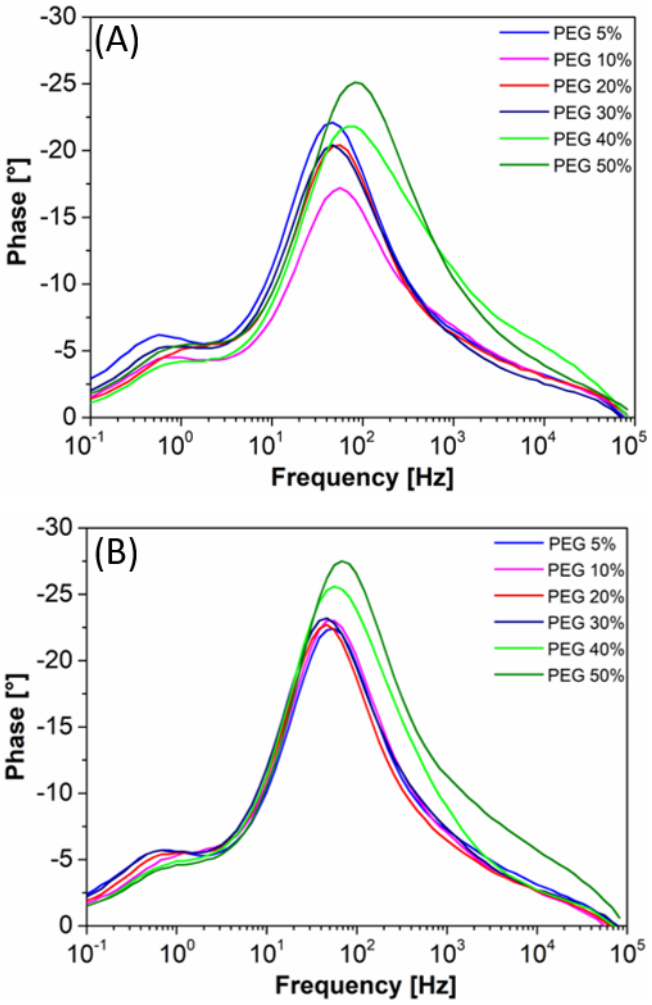

Figure 9. Bode's plot of (A) liquid and (B) quasi-solid state aqueous DSSCs assembled with photoanodes obtained from different PEG-based pastes. Spectra were recorded under 1 sun irradiation.

Conclusion

Amelioration of the morphological and electronic properties of TiO_2 photoanodes is a key aspect for improving efficiency of DSSCs, especially the emerging water-based ones. The effects of such modification can lead to an improvement of the interface between TiO_2 and electrolyte, the suppression of charge recombination and/or a better electron injection efficiency from the dye to the semiconductor. In this work, we investigated the effects of the addition of several polymeric and molecular compounds to a commercial TiO_2 paste, deposited by doctor blading on FTO glasses. It was proved that, among others, PEG showed an appreciable positive effect on PV parameters when

both liquid and quasi-solid state aqueous electrolytes were used. The pristine TiO_2 paste was then mixed with different PEG amounts in order to precisely studying the effect of such an additive on morphology, structure, thickness and (photo)electrochemical properties of the resulting photoanodes and cells. The addition of PEG led to a sensible modification of the electrode thickness and its morphology: the higher the amount of PEG in the paste, the bigger the void spaces within the semiconductor film. The best PV performance was obtained using the paste containing PEG 20 wt%, achieving a PCE of 2.3% with both liquid and hydrogel electrolytes. Interestingly, devices fabricated with the XG electrolyte showed longer stability with respect to their liquid counterparts, and the aging test was carried out for more than 80 days. EIS was employed as an effective tool to investigate the effect of PEG amount on the electrochemical phenomena in cell components and at their interfaces; the most efficient device showed the longest electron lifetime coupled to a smaller electron transport resistance.

Overall, PEG was proved to be an effective additive to improve the properties of TiO_2 photoanodes for aqueous DSSCs, suggesting that the currently commercially available printable pastes can be used in this field after proper modifications. This constitutes an important aspect in view of a DSSCs industrial production chain, where aqueous systems can markedly increase the product features in terms of safety, environmental friendliness and costs, without losing the know-how developed in the last 25 years with organic solvents-based cells.

Acknowledgements

The authors cordially thank CNIS and Dr. Francesco Mura (for EDX measurements) and Dr. Chiara Riedo (for the technical support in rheological analysis). Politecnico di Torino is gratefully acknowledged by F.B. for granting the fund named “Contributo ERC per chi ha superato il primo step di valutazione”. M.B. and C.B. wish to acknowledge the financial support from the European Union Horizon 2020 research and innovation program under grant agreement no. 826013 (IMPRESSIVE).

References

[1] a) Y. Matsuo, S. Endo, Y. Nagatomi, Y. Shibata, R. Komiyama, Y. Fujii, *Appl. Energy* **2020**, *267*, 113956; b) A. Genus, M. Iskandarova, *Renewable Sustainable Energy Rev.* **2020**, *125*, 109795; c) S. J. Varma, K. Sambath Kumar, S. Seal, S. Rajaraman, J. Thomas, *Adv. Sci.* **2018**, *5*, 1800340; d) T. M. W. J. Bandara, L. A. DeSilva, J. L. Ratnasekera, K. H. Hettiarachchi, A. P. Wijerathna, M. Thakurdesai, J. Preston, I. Albinsson, B. E. Mellander, *Renewable Sustainable Energy Rev.* **2019**, *103*, 282-290; e) S. Sasi, S. K. Sugunan, P. Radhakrishnan Nair, K. R. V. Subramanian, S. Mathew, *Photochem. Photobiol. Sci.* **2019**, *18*, 15-29.

[2] a) A. Jäger-Waldau, I. Kougias, N. Taylor, C. Thiel, *Renewable Sustainable Energy Rev.* **2020**, *126*, 109836; b) M. Alipour, H. Salim, R. A. Stewart, O. Sahin, *Renewable Sustainable Energy Rev.* **2020**, *123*, 109749; c) Y. Guo, T. Zou, Q. Cheng, B. Jiao, X. Zhang, *J. Wuhan Univ. Technol.* **2019**, *34*, 17-22; d) K. A. Kumar, K. Subalakshmi, J. Senthilselvan, *Mater. Sci. Semicond. Process.* **2019**, *96*, 104-115; e) H. Kusama, *J. Photochem. Photobiol., A* **2019**, *376*, 255-262.

[3] a) M. Grätzel, *J. Photochem. Photobiol., C* **2003**, *4*, 145-153; b) G. R. Li, X. P. Gao, *Adv. Mater.* **2020**, *32*, 1806478; c) J. M. Cole, G. Pepe, O. K. Al Bahri, C. B. Cooper, *Chem. Rev.* **2019**, *119*, 7279-7327; d) K. Sun, Y. Liu, Y. Wu, X. Guo, J. Li, L. Wang, *J. Mol. Liq.* **2019**, *278*, 484-490; e) F. Hu, W. Liu, W. Li, Z. Xu, Y. Y. Diao, N. B. Lin, W. Guo, L. Shi, J. H. van Esch, X. Y. Liu, *Small* **2019**, *15*, 1804171.

[4] a) H. Yuan, W. Wang, D. Xu, Q. Xu, J. Xie, X. Chen, T. Zhang, C. Xiong, Y. He, Y. Zhang, Y. Liu, H. Shen, *Sol. Energy* **2018**, *165*, 233-239; b) G. Li, L. Sheng, T. Li, J. Hu, P. Li, K. Wang, *Sol. Energy* **2019**, *177*, 80-98; c) "Dye Sensitized Solar Cell Market Size, Share & Trends Analysis Report by Application (Portable Charging, BIPV/BAPV, Embedded Electronics, Outdoor Advertising, Automotive (AIPV)), and Segment Forecasts, 2015–2022", https://www.grandviewresearch.com/industry-analysis/dye-sensitized-solar-cell-market, by Grand View Research, Inc., accessed August 2020.

[5] B. O'Regan, M. Grätzel, *Nature* **1991**, *353*, 737-740.

[6] K. Kakiage, Y. Aoyama, T. Yano, K. Oya, J. I. Fujisawa, M. Hanaya, *Chem. Commun.* **2015**, *51*, 15894-15897.

[7] "Best Research-Cell Efficiency Chart", by The National Renewable Energy Laboratory, https://www.nrel.gov/pv/cell-efficiency.html, accessed August 2020.

[8] a) N. Mariotti, M. Bonomo, L. Fagiolari, N. Barbero, C. Gerbaldi, F. Bella, C. Barolo, *Green Chem.* **2020**, DOI: 10.1039/D0GC01148G; b) M. Colovic, J. Volavšek, E. Stathatos, N. Celan Korošin, M. Šobak, I. Jerman, *Sol. Energy* **2019**, *183*, 619-631; c) A. Miguel, F. González, V. Gregorio, N. García, P. Tiemblo, *Polymers* **2019**, *11*, 406; d) N. M. Saidi, H. Ming Ng, F. S. Omar, S. Bashir, K. Ramesh, S. Ramesh, *J. Appl. Polym. Sci.* **2019**, *136*, 47810; e) N. F. Zain, N. A. Dzulkurnain, A. Ahmad, F. Salleh, N. S. Mohamed, *J. New Mater. Electrochem. Syst.* **2019**, *22*, 65-69.

[9] a) F. Bella, C. Gerbaldi, C. Barolo, M. Grätzel, *Chem. Soc. Rev.* **2015**, *44*, 3431-3473; b) F. Bella, S. Galliano, M. Falco, G. Viscardi, C. Barolo, M. Grätzel, C. Gerbaldi, *Chem. Sci.* **2016**, *7*, 4880-4890; c) M. Khalili, M. Abedi, H. S. Amoli, S. A. Mozaffari, *Carbohydr. Polym.* **2017**, *175*, 1-6.

[10] a) W. Xiang, D. Chen, R. A. Caruso, Y. B. Cheng, U. Bach, L. Spiccia, *ChemSusChem* **2015**, *8*, 3704-3711; b) F. Bella, S. Galliano, M. Falco, G. Viscardi, C. Barolo, M. Grätzel, C. Gerbaldi, *Green Chem.* **2017**, *19*, 1043-1051.

[11] a) Z. S. Wang, H. Kawauchi, T. Kashima, H. Arakawa, *Coord. Chem. Rev.* **2004**, *248*, 1381-1389; b) S. Ito, P. Chen, P. Comte, M. K. Nazeeruddin, P. Liska, P. Péchy, M. Grätzel, *Prog. Photovoltaics Res. Appl.* **2007**, *15*, 603-612; c) J. R. Jennings, A. Ghicov, L. M. Peter, P. Schmuki, A. B. Walker, *J. Am. Chem. Soc.* **2008**, *130*, 13364-13372; d) R. Iacobellis *et al.*, *Sci. Rep.* **2016**, *6*, 39509; e) S. K. Arla, S. S. Sana, V. Badineni, V. K. N. Boya, *Bull. Mater. Sci.* **2020**, *43*, 210.

[12] C. Dong, W. Xiang, F. Huang, D. Fu, W. Huang, U. Bach, Y. B. Cheng, X. Li, L. Spiccia, *Angew. Chem. Int. Ed.* **2014**, *53*, 6933-6937; *Angew. Chem.* **2014**, *126*, 7053-7057.

[13] Y. Guo, T. Zou, Q. Cheng, B. Jiao, X. Zhang, *J. Wuhan Univ. Technol.-Mat. Sci. Edit.* **2019**, *34*, 17-22.

[14] H. J. Son, C. Prasittichai, J. E. Mondloch, L. Luo, J. Wu, D. W. Kim, O. K. Farha, J. T. Hupp, *J. Am. Chem. Soc.* **2013**, *135*, 11529-11532.

[15] S. Galliano, F. Bella, M. Bonomo, G. Viscardi, C. Gerbaldi, G. Boschloo, C. Barolo, *Nanomaterials* **2020**, *10*, 1585.

[16] S. Sapino *et al.*, *Nanomaterials* **2019**, *9*, 1461.

[17] a) S. J. Park, K. Yoo, J. Y. Kim, J. Y. Kim, D. K. Lee, B. Kim, H. Kim, J. H. Kim, J. Cho, M. J. Ko, *ACS Nano* **2013**, *7*, 4050-4056; b) A. Syairah, M. H. Khanmirzaei, N. M. Saidi, N. K. Farhana, S. Ramesh, K. Ramesh, S. Ramesh, *Ionics* **2019**, *25*, 2427-2435; c) S. Santhaveesuk, S. Pukird, C. Kahattha, *Mater. Today:. Proc.* **2018**, *5*, 14086-14090; d) S. Venkatesan, I. P. Liu, W. N. Hung, H. Teng, Y. L. Lee, *Chem. Eng. J.* **2019**, *367*, 17-24; e) F. Bella, J. R. Nair, C. Gerbaldi, *RSC Adv.* **2013**, *3*, 15993-16001; f) A. Scalia, F. Bella, A. Lamberti, C. Gerbaldi, E. Tresso, *Energy* **2019**, *166*, 789-795.

[18] J. G. Nam, E. S. Lee, W. C. Jung, Y. J. Park, B. H. Sohn, S. C. Park, J. S. Kim, J. Y. Bae, *Mater. Chem. Phys.* **2009**, *116*, 46-51.

[19] D. K. Kumar, S. K. Swami, V. Dutta, B. Chen, N. Bennett, H. M. Upadhyaya, *FlatChem* **2019**, *15*, 100105.

[20] S. Kiran, S. K. Naveen Kumar, K. C. Yogananda, D. Rangappa, *J. Mater. Sci. - Mater. Electron.* **2018**, *29*, 12681-12689.

[21] M. F. Aziz, I. M. Noor, B. Sahraoui, A. K. Arof, *Opt. Quantum Electron.* **2014**, *46*, 133-141.

[22] O. Rynne, M. Dubarry, C. Molson, D. Lepage, A. Prébé, D. Aymé-Perrot, D. Rochefort, M. Dollé, *Batteries* **2019**, *5*, 72.

[23] Y. Masuda in *Nanofabrication* (Ed.: Y. Masuda), IntechOpen, Rijeka, **2011**, chapter 1.

[24] V. R. Almeida, Q. Xu, C. A. Barrios, M. Lipson, *Opt. Lett.* **2004**, *29*, 1209-1211.

[25] H. Michaels, M. Rinderle, R. Freitag, I. Benesperi, T. Edvinsson, R. Socher, A. Gagliardi, M. Freitag, *Chem. Sci.* **2020**, *11*, 2895-2906.

[26] V. Leandri, H. Ellis, E. Gabrielsson, L. Sun, G. Boschloo, A. Hagfeldt, *Phys. Chem. Chem. Phys.* **2014**, *16*, 19964-19971.

[27] a) H. Tian, E. Gabrielsson, P. W. Lohse, N. Vlachopoulos, L. Kloo, A. Hagfeldt, L. Sun, *Energy Environ. Sci.* **2012**, *5*, 9752-9755; b) S. Zhang, G. Y. Dong, B. Lin, J. Qu, N. Y. Yuan, J. N. Ding, Z. Gu, *Sol. Energy* **2016**, *127*, 19-27.

[28] H. Choi, B. S. Jeong, K. Do, M. J. Ju, K. Song, J. Ko, *New J. Chem.* **2013**, *37*, 329-336.

[29] A. Hauch, A. Georg, *Electrochim. Acta* **2001**, *46*, 3457-3466.